Numerical Study of Confined Explosions in Urban Environments

by

Ramón H. Codina, Daniel Ambrosini, Fernanda de Borbón

Reprinted from
International Journal of
Protective Structures

Volume 4 · Number 4 · December 2013

Multi-Science Publishing
ISSN 2041-4196

Numerical Study of Confined Explosions in Urban Environments

Ramón H.Codina[1,2], Daniel Ambrosini[1,2*], Fernanda de Borbón[1,2]
[1]Structural Engineering Master Program, Engineering Faculty, National University of Cuyo, Centro Universitario, Parque General San Martín, 5500 Mendoza, Argentina
[2]National Research Council CONICET, Argentina

ABSTRACT
In recent years, events such as the attack on the World Trade Center as well as many other attacks around the world have shown that terrorism-related activity is dramatically increasing. Such a situation makes necessary to study the effects of blast loading on complex urban environments. In this paper, the phenomenon of channelling in congested urban environments is studied. Channelling is a phenomenon that can significantly increase the destructive potential of a shock wave of an explosion. Hence, channelling must be taken into account in the design of structures subjected to extreme loads in congested urban environments. This paper presents a novel approach to understanding channelling effects using maps of overpressure amplification and impulse amplification. These maps are developed for different street widths and amounts and locations of explosive loads and could be used as a first approximation for design purposes. The characteristic channelling zones are defined and characterised for the first time in the open technical literature. Finally, quantitative conclusions about the influence of the different parameters are highlighted.

Keywords: Blast Waves, Street Channelling, Canyon Effect, Confined Explosions, Urban Settings

1. INTRODUCTION

For the last few decades, the effects of blast loading on structures have been studied by many researchers around the world. Such explosions can be caused by events such as industrial accidents or terrorist attacks. It is therefore important to develop tools for the determination of design parameters and methods to improve the performance of structures that may be subjected to blast loads.

Historically, simplified analytical models and empirical methods, such as those found in technical manuals (UFC 3-340-02 [1] – TM5-855-1 [2]) or software such as CONWEP [3], were used to solve this type of problem. Some of these methods can be found in classical books, i.e., Baker et al. [4], Smith and Hetherington [5], or Cormie et al. [6]. However, these simplified tools are not able to solve problems with complex geometries where there are multiple blast wave reflections.

*Corresponding author. E-mail: dambrosini@uncu.edu.ar

With the development of computer hardware over the last decades, it has become possible to perform numerical simulations of explosive events using personal computers. This was significantly enhanced by the development of numerical methods such as the Godunov scheme and Flux Corrected Transport (FCT) algorithms, which have enabled the development of more efficient hydrocodes to solve problems related to the fluid dynamics of shock waves. Hydrocodes are a useful tool for analysing such events and can be performed with various strategies. Clutter et al. [7] and Johansson et al. [8] showed good correlation between numerical and experimental results. Larcher and Casadei [9] presented several methods for simulating air blast waves, which can also be used within complex structures.

At present, there is a deep physical and chemical understanding of the phenomena involved in a detonation that can be reproduced using hydrocodes (Alia and Souli [10]; Alhussan et al. [11]). The development of these techniques has allowed the use of complex models that can solve the problem of soil structure interaction (SSI) in buried structures subjected to blast loadings (Lu et al. [12]; Wang et al. [13]) or the air-structure interaction (Børvik et al. [14]; Luccioni et al. [15]). Moreover, Johasson et al. [8], Rose and Smith, [16] Trélat et al. [17], and Zyskowski et al. [18] have shown that it is possible to obtain reliable and accurate results from numerical modelling by comparing numerical results to results from experimental testing.

On the other hand, the study of blast loadings on confined spaces such as tunnels is receiving increasing attention from structural engineers. The confinement of an explosion increases the magnitudes of overpressures and impulses due to successive reflections against the obstacles encountered by the blast wave. Rigas and Sklavounos [19] performed a comparison between a numerical model made with CFX-5.6 code and experimental tests. Benselama et al. [20] performed a parametric study on this topic, and Silvestrini et al. [21] proposed a simplified method for estimating the overpressures from blast waves.

2. STREET CHANNELLING

The study of explosions in complex urban environments has been approached by many researchers. Remennikov [22] presented a review of methods for predicting bomb blast effects on buildings that are essentially isolated. In congested urban environments, confinement effects also occur. This is usually referred to in the literature as “street channelling”, “channelling” or the “canyon effect” [16, 23]. The buildings façades and other obstacles interrupt the propagation of the blast waves, which generates wave reflections and combinations of incident and reflected waves.

The prediction of blast wave characteristics becomes more difficult with increasing interactions between the number of buildings in the urban (or suburban) environment and the propagated blast wave front. Smith and Rose [24] presented an overview of research conducted both experimentally and analytically in the area of blast wave interactions with buildings and structures in an urban landscape. Rose and Smith [16] studied the effects of confinement induced by tall buildings that border straight city streets on the positive and negative phase impulses of blast waves originating from explosive detonations. It was determined that positive phase blast wave impulses can be enhanced by a factor of five or more in narrow city streets compared to side-on values at equivalent distances. It was also demonstrated that the negative phase impulse becomes increasingly important in an urban setting because of the large expansion that occurs when the blast wave reaches the top of a building or the end of the street. Fairlie et al. [25] experimentally evaluated the channelling of a blast wave in crossroads geometry and compared the experimental and numerical pressures and impulses with the results predicted by AUTODYN; good agreement was

obtained between the numerical and experimental results. Ambrosini et al. [26] and Luccioni et al. [27] studied the propagation of blast waves in an urban environment to determine the mass of explosives used in a terrorist attack. Benselama et al. [20] showed that this type of study can be used to draw P-I iso-damage diagrams. Regarding the numerical tool, AUTODYN was used in [25-27] and Air3D in [16, 23-24].

The aim of this paper is to study the effects of channelling of shock waves in urban areas through a numerical parametric study. To achieve this objective, the variations of different parameters, such as explosive amounts, explosive location and street width, are analysed. The parametric study allows the channelling effects to be presented in in a novel way using maps of the overpressure and impulse amplifications. In most papers, it is not determined whether the enhancement of the overpressures and impulses is produced by reflection, a Mach effect or the channelling itself. In this paper, the maps of overpressure and impulse amplification show four types of zones where the channelling effects are different and the characteristics of each zone are discussed. Further, an analysis of the effects on the channelling phenomenon of an asymmetric explosive charge located at 2.20 meters from one of the façades, which is the width of a typical sidewalk, is presented. Finally, quantitative conclusions about the influence of the different parameters are highlighted.

3. PARAMETRIC STUDY

The weights of the explosive loads used in the analysis were 100, 500, 1,000, 5,000 and 10,000 kg of equivalent TNT. These amounts of explosives were chosen because these amounts can be found in different types of improvised explosive devices (IEDs), such as cars, vans and even trucks (FEMA 426 [28]). Additionally, the most representative street widths in European cities, such as Paris, Madrid and Rome, were studied. It was concluded that the most representative widths were 6, 12 and 20 meters [29]. In all cases, the space studied was 100 meters long (the length of a typical block) by the widths considered. The height adopted for the models was 20 meters, which is a representative height of the buildings in the cities used as examples [29]. The buildings were modelled as rigid surfaces that allow the complete reflection of shock waves. This assumption is discussed in section 4.3.

The explosive was modelled as a sphere of TNT with its lower bound suspended 1 m above the ground. Moreover, the explosive was considered to be located at one of two positions: centred on the street axis and located at 2.20 meters from one of the façades, which is the width of a typical sidewalk. The first case was called a symmetric explosion, and the second case was called an asymmetric explosion (Figure 1). Due to the symmetry of the problem, only a quarter of the space was modelled for the first case, and half of the space was modelled for the second case.

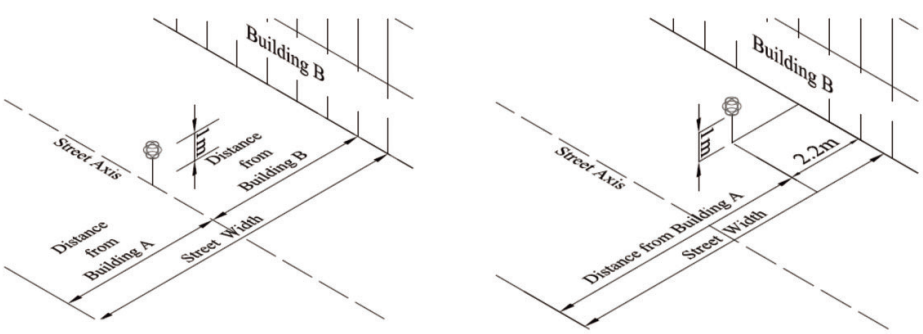

Figure 1. Locations of explosive on the street: a) Symmetric explosions, b) Asymmetric explosions

4. NUMERICAL MODELS

Computer codes normally referred as "hydrocodes" encompass several different numerical techniques to solve a wide variety of non-linear problems in solid, fluid and gas dynamics. The phenomena to be studied with such programs can be characterised as highly time dependent with both geometric non-linearities (i.e., large strains and deformations) and material non-linearities (i.e., plasticity, failure, strain-hardening and softening, multiphase equations of state). In this paper, the ANSYS-AUTODYN [30] hydrocode was used through an Euler multimaterial processor.

4.1 MATERIAL MODELS

The air was modelled as an ideal gas. This may be derived from the laws of Boyle and Gay-Lussac (ANSYS-AUTODYN [30]), given by Equation (1):

$$p = (\gamma - 1)\rho e \tag{1}$$

where p is the hydrostatic pressure, γ is the adiabatic constant, ρ is air density, and e is the specific internal energy.

Table 1 shows the properties of the air used in this study.

Table 1. Properties of air

g	ρ [kg/cm^3]	θ [K]	cv [J/kgK]	e [KJ/m^3]
1.4	1.223e-6	288.2	717.6	2.068e5

where θ is the temperature and cv is the specific heat.

The explosive is modelled using the "Jones-Wilkins-Lee" (JWL) equations of state [31]. This equation correctly reproduces the phenomenon of the expansion of gases after detonation:

$$p = C_1\left(1 - \frac{\omega}{r_1 v}\right)e^{-r_1 v} + C_2\left(1 - \frac{\omega}{r_2 v}\right)e^{-r_2 v} + \frac{\omega e}{v} \tag{2}$$

$$v = 1/\rho \tag{3}$$

where ρ is the explosive density; A, B, R_1, R_2 and ω are the JWL adjustments parameters; and γ is the adiabatic constant.

The TNT properties used in this study are shown in Table 2.

Table 2. TNT properties (EOS JWL)

ρ [g/cm^3]	A [KPa]	B [KPa]	R_1	R_2	ω	$V_{C\text{-}J}$ [m/s]	$e_{c\text{-}j}$ [KJ/m^3]	$p_{C\text{-}J}$ [KPa]
1.63	3.7377e+8	3.7471e+6	4.15	0.90	0.35	6.93e+3	6.0e+6	2.1e+7

where $V_{C\text{-}J}$ is the C-J detonation velocity.

4.2 MESH VALIDATION AND REMAPPING

The accuracy of numerical results is strongly dependent on the mesh size used for the analysis. Luccioni et al. [32] compared numerical models with experimental results and

concluded that a 100-mm mesh is accurate enough for the analysis of wave propagation in urban environments. Nevertheless, it may be too computationally expensive to model a complete block using this mesh size. Alternatively, a coarser mesh can be used to obtain results with acceptable accuracy. Moreover, the minimum cell size can be influenced by the available computational and time resources. The use of coarse meshes is common in this type of study because of the size of the models and the limited computational capacity. Ambrosini et al. [26], Luccioni et al. [27] and Remennikov [22] used cells of 500 mm; Remennikov and Rose [23] used cells of 300 mm; and Zhou and Hao [33] used a mesh size of 250 mm.

A reduced but representative model of the problem under study was performed (Figure 2). The model has a 6-m street width with an asymmetric explosion of 100 kg of TNT. To study the mesh sensitivity and calibrate the accuracy of the numerical results, three different element sizes were considered: 500, 250 and 125 mm.

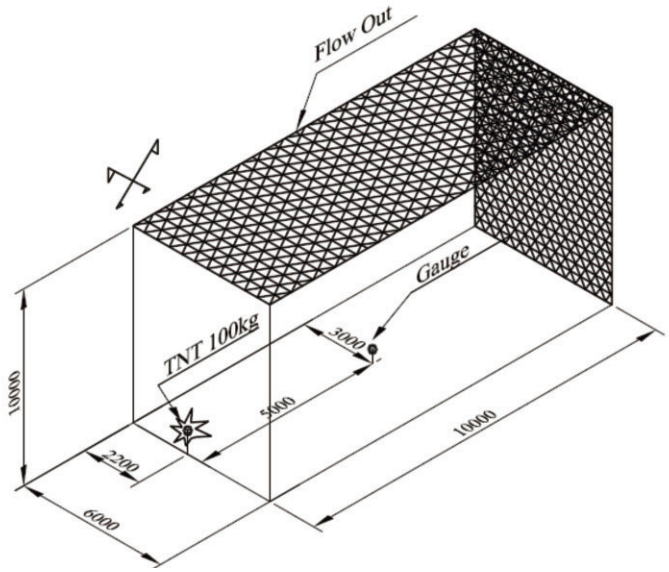

Figure 2. Model for the study of mesh sensitivity

Figure 3 shows the pressure-time history and impulse-time history curves obtained for a gauge located at 5 m from an explosive charge of 100 kg of TNT (Figure 2). There are noticeable differences among the peak overpressures obtained for the different mesh sizes. It must be noted that, as the mesh is refined, the difference between the results for the different mesh sizes is reduced, demonstrating the convergence of numerical results. The coarse mesh model fails to capture the very sharp peak of the blast wave. Further reduction of the element size will result in a better estimation of peak pressures but will substantially increase the computational time. On the other hand, the impulses show good accuracy even with the coarser mesh.

While the difference between the estimated peak overpressure for mesh sizes of 125 and 500 mm is approximately 32%, the difference between the estimated peak overpressure for mesh sizes of 125 and 250 mm is approximately 17%. The comparison of maximum impulses shows that the difference between the estimated maximum impulse for mesh sizes of 125 and 500 mm is approximately 8.3%, and the difference for mesh sizes of 125 and 250

mm is approximately 3%. Because a very sharp peak overpressure has little effect on structures and a very good estimation of impulses is obtained using the mesh size of 250 mm, the mesh size of 250 mm is selected in the present study to carry out the numerical simulations.

In this study, a 1D model is used to reproduce the first phase of the explosion. At this stage, blast waves do not reach the ground or the walls of the buildings. The second phase of the explosion takes place in a two-dimensional space where the soil is a reflective barrier. This phase ends just before the pressure wave reaches a side wall. After that, the third phase is the development of a three-dimensional shock wave. Moving from one phase to the next requires remapping (Luccioni et al. [15]; Benselama et al. [34]).

The dimensions of the 3D models are presented in Table 3.

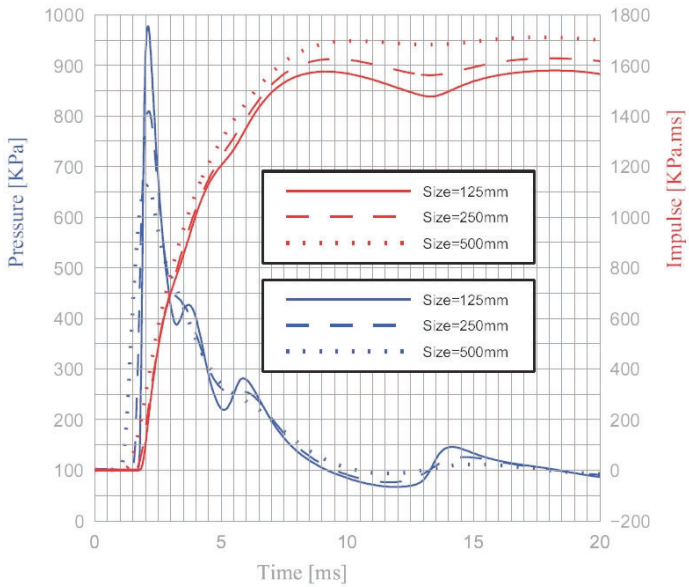

Figure 3. Mesh sensitivity

Table 3. 3D model dimensions

	Street Width [m]	B [m]	H [m]	L [m]	Δx [mm]	Δy [mm]	Number of Cells
Symmetric	6	3	20	50	1023	300	192000
	12	6	20	50	1500	400	384000
	20	10	20	50	2045	500	640000
Asymmetric	6	6	20	50	1216	500	384000
	12	12	20	50	2045	600	768000
	20	20	20	50	2045	1000	1280000

where B is the distance from the axis of the street to the wall for the symmetric model or the total street width for the asymmetric model; H is the height of the adopted model; and Δx and Δy are the adopted spacings of the gauges.

The symmetric and asymmetric 3D model dimensions are shown in Figure 4.

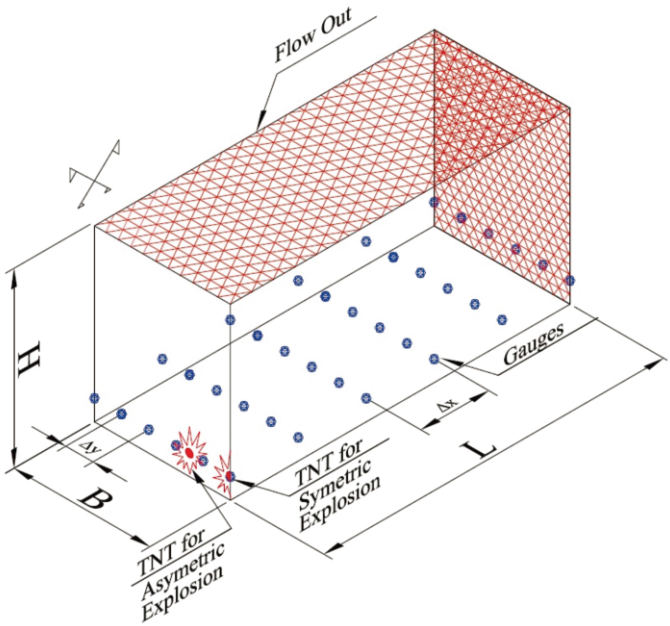

Figure 4. 3D models

4.3 BOUNDARY CONDITIONS

Two types of boundary conditions were used: rigid reflecting surfaces and transmitting boundaries (flow-out). The first one reflects the total of the incident shock waves, and it is simply defined by the boundary of the Euler mesh. The second one allows the waves to be transmitted through them, out of the model.

The rigid reflecting surfaces were used to represent the building façades and the ground, while flow-out surfaces were used to model the areas where the waves escape from the confined area at the top of the model and the end of the block.

The assumption of the façades of buildings as rigid surfaces may constitute a limitation of this methodology because it leads to an overestimation of the pressures and impulses. Actually, part of the energy generated by the explosion is dissipated in the process of destructing structures and materials. However, if the building façades do not fail, the transfer of momentum to the building is small, and the rigid assumption is valid [23]. In fact, this assumption is well supported by experiments where the buildings are modelled using rigid blocks and plates [35].

On the other hand, it is important to emphasise that this paper presents a comparative study, and for this reason, the energy dissipated in the cratering process is the same in both cases. Moreover, if the blast wave destroys the façades of nearby buildings, the wave will not normally pass indefinitely but will be reflected some meters inside [15], and the time in the enhancing of the incident wave can be considered negligible. Generally, it is necessary to find a balance between accuracy and computational cost, and the hypothesis of rigid surfaces is normally used in this type of study [22-24; 26-27; 36]. The consequences of the hypothesis

of rigid surfaces on the blast propagation along city streets were studied deeply by Smith et al. [37]. Finally, it should be highlighted that this assumption results in conservative estimations.

4.5 CONFINED AND UNCONFINED 3D MODELS

Because the objective of this paper is to compare the overpressures and impulses generated by confined and unconfined explosions, a 3D unconfined model was built. In the unconfined model, the gauges maintain the same relative location to the explosive than in the confined model. The unconfined model has a volume of 50 m x 50 m x 20 m and a total of 3.2 million cells. In all cases, the gauges were placed in a horizontal plane 1 m above the ground level. The confined and unconfined 3D models are shown in Figure 5.

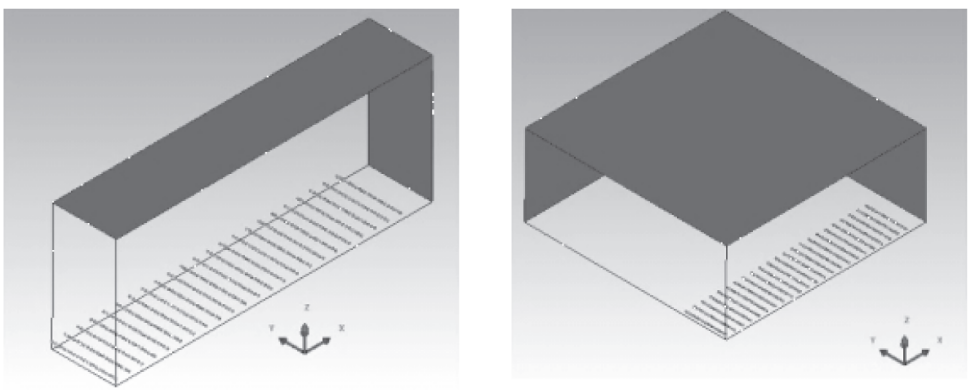

(a) (b)

Figure 5. Confined and unconfined 3D models: a) Confined 3D models; b) Unconfined 3D models

5. RESULTS

As stated earlier, the building façades and the ground interrupt the propagation of the blast waves, generating wave reflections and combinations of incident and reflected waves. The effects of confinement on the overpressures and impulses are studied. These are design parameters which are usually used to estimate the destructive potential of an explosion. To clearly display the channelling phenomenon, amplification maps are performed. The maps show the channelling on a horizontal plane one meter above ground level covering the entire surface of the street.

5.1 OVERPRESSURES AMPLIFICATION

This section presents the amplification maps of the maximum overpressures recorded at the gauge points. They were obtained from the overpressure records of an explosion for confined and unconfined models. The overpressure amplification is obtained as

$$PA = \frac{PC}{PSC} \tag{4}$$

where *PA* is the overpressure amplification coefficient, *PC* is the maximum overpressure recorded at a gauge in the confined model, and *PSC* is the maximum overpressure recorded at the same gauge in the equivalent unconfined model. The *PA* maps for different street widths and different amounts of explosive are shown in Figures 6 to 8. In these figures, symmetrical explosions are plotted on the left side and asymmetrical explosions on the right. This enables a comparison of how the confinement zones differ with the location of the explosive.

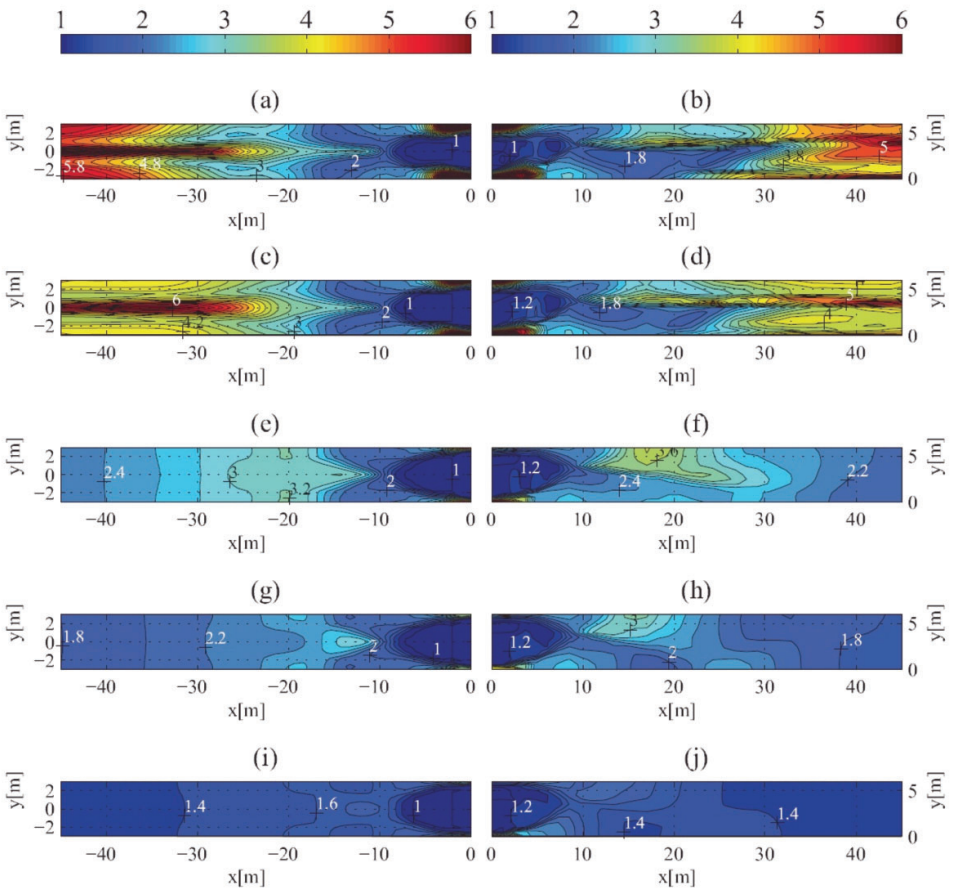

Figure 6. PA maps, streets 6 meters wide: a) and b) 10,000 kg of TNT; c) and d) 5,000 kg of TNT; e) and f) 1,000 kg of TNT; g) and h) 500 kg of TNT; i) and j) 100 kg of TNT

In the area near the explosives, the overpressure amplification is close to 1; therefore, the channelling effect does not affect the maximal overpressure value in this area. For this reason, it is proposed to call this zone as *Unconfined Area*. In this area, no overlap between reflected and incident waves is produced; hence, the maximum pressure recorded by the gauge is always the incident pressure, which is the same for the confined and unconfined explosions. This *Unconfined Area* is found in both the symmetric and asymmetric explosions, and it does not change with the amount of explosive. The Mach effect against the

façades shapes the unconfined zone. The zones in which the amplification is dominated by the Mach effect are named *Mach Reflection Area*. Finally, the remaining two areas are the *Regular Reflection Area* in which the amplification is dominated by the reflection on the walls and the *Confined Area* in which the channelling effect enhances the blast wave. When the street is wider, the amplification factors are reduced along the street, and consequently, the shapes of the different channelling zones are strongly dependent on the dimensions of the street.

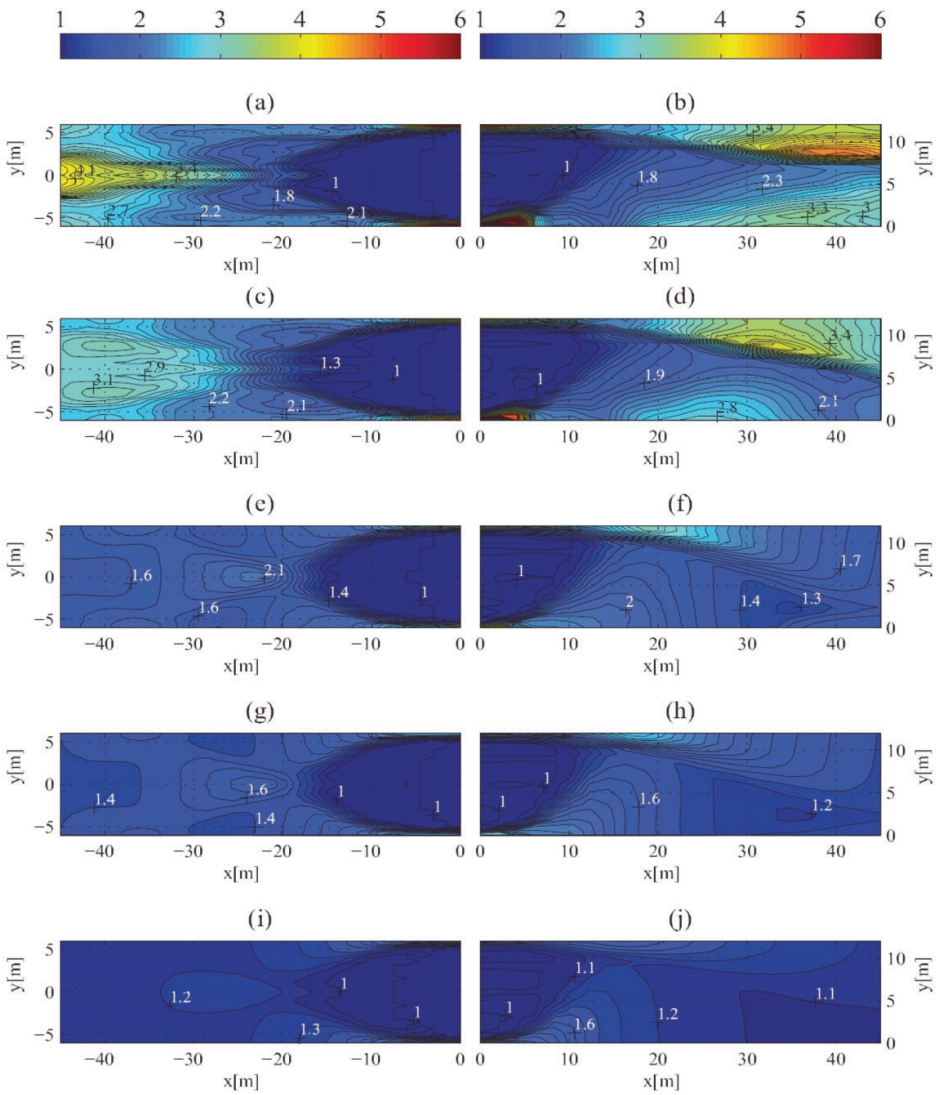

Figure 7. *PA* maps, streets 12 meters wide: a) and b) 10,000 kg of TNT; c) and d) 5,000 kg of TNT; e) and f) 1,000 kg of TNT; g) and h) 500 kg of TNT; i) and j) 100 kg of TNT

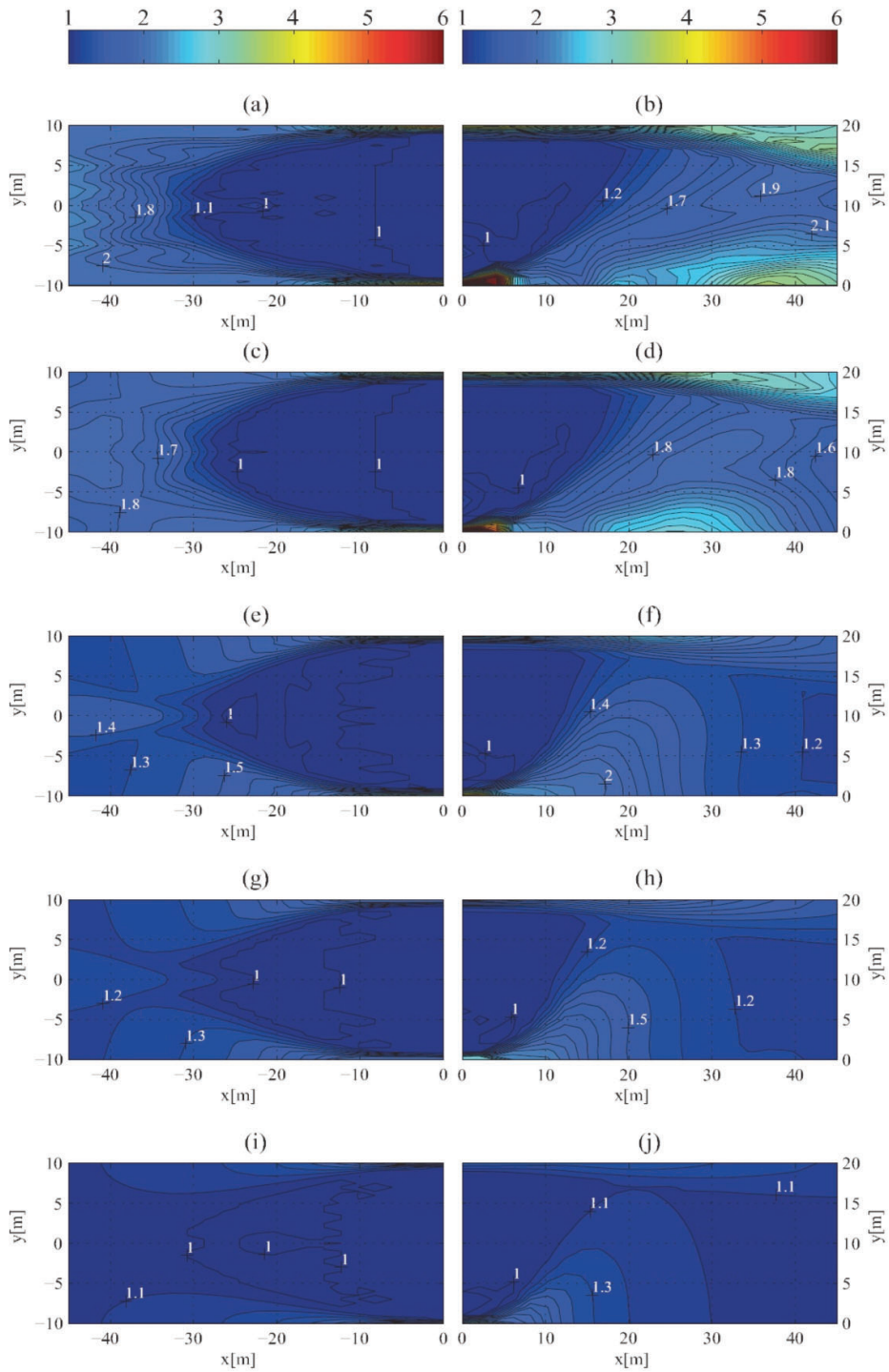

Figure 8. *PA* maps, streets 20 meters wide: a) and b) 10,000 kg of TNT; c) and d) 5,000 kg of TNT; e) and f) 1,000 kg of TNT; g) and h) 500 kg of TNT; i) and j) 100 kg of TNT

5.2 Impulse amplification

This section presents the amplification maps of the maximum impulses recorded at the gauge points. They were obtained from the impulse records of an explosion for confined and unconfined models. The impulse amplification is obtained as

$$IA = \frac{IC}{ISC} \tag{5}$$

where *IA* is the impulse amplification coefficient, *IC* is the maximum impulse recorded at a gauge from the confined model, and *ISC* is the maximum impulse recorded at the same gauge in the equivalent unconfined model. The *IA* maps for different street widths and different amounts of explosive are shown in Figures 9 to 11. These maps show the effects of channelling on a horizontal plane at one meter above the street. In these figures, the symmetrical explosions are plotted on the left side, and asymmetrical explosions are plotted on the right. This allows a visualisation of how the confinement zones differ with the location of the explosive.

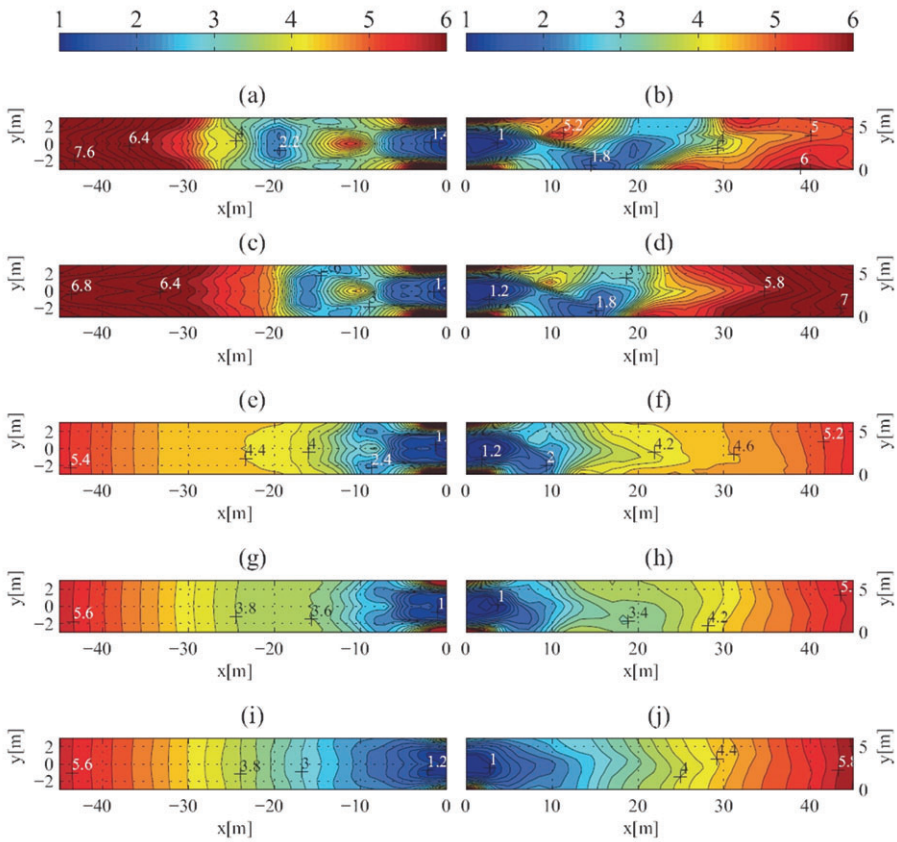

Figure 9. *IA* maps, streets of 6 meters wide: a) and b) 10,000 kg of TNT; c) and d) 5,000 kg of TNT; e) and f) 1,000 kg of TNT; g) and h) 500 kg of TNT; i) and j) 100 kg of TNT

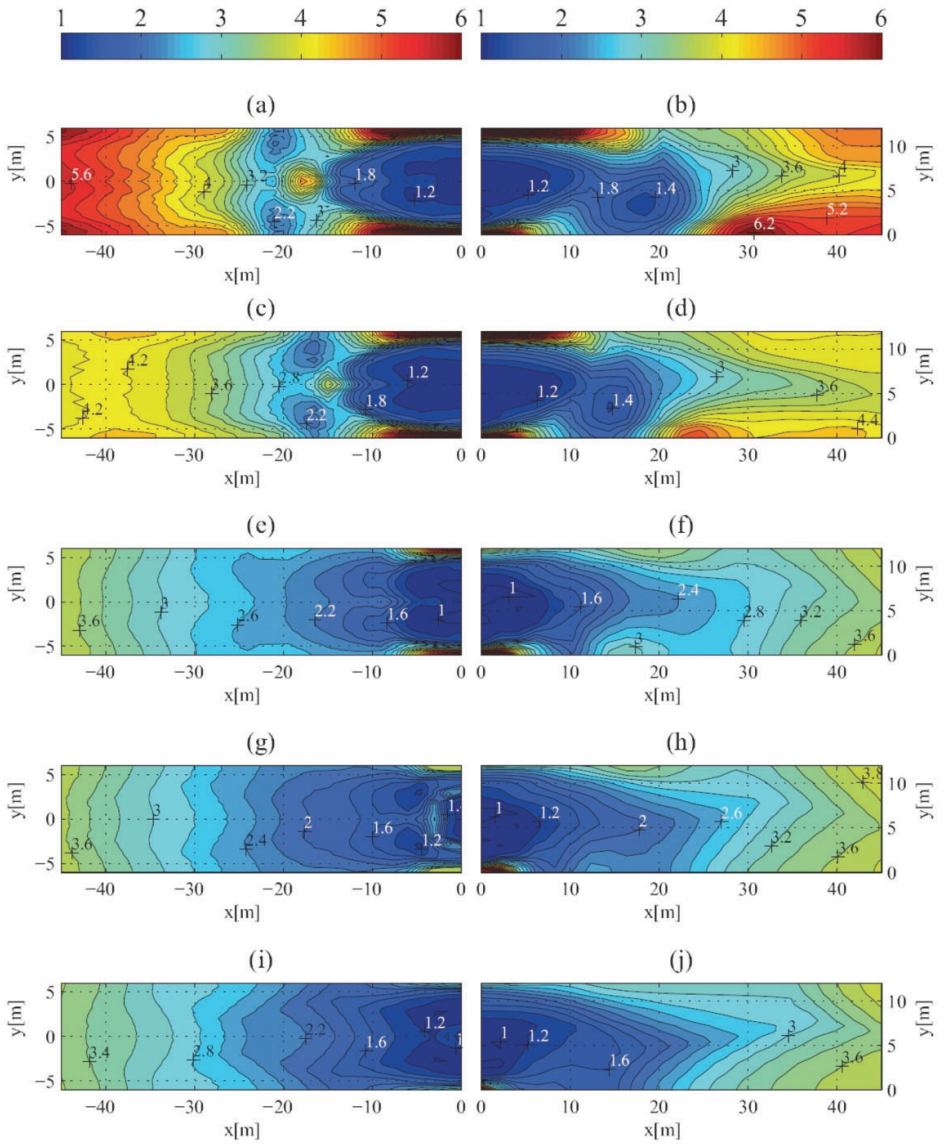

Figure 10. *IA* maps, streets 12 meters wide: a) and b) 10,000 kg of TNT; c) and d) 5,000 kg of TNT; e) and f) 1,000 kg of TNT; g) and h) 500 kg of TNT; i) and j) 100 kg of TNT

As shown in Figures 9 to 11, the impulse amplification maps are different to the overpressure amplification maps in several respects (Figures 6 to 8). The main difference is that, in the area near the explosive, impulse amplification is observed. This is due to the cumulative nature of the impulse, which does not need the combination of incident and reflected waves to increase its value compared to the unconfined explosion. Aside from this difference, the same areas swept by the Mach wavefront are distinguished in these maps; hence, the four zones found in the overpressure maps can be observed in these maps. As in the *PA* maps, when the street is wider, the amplification factors decrease along the street.

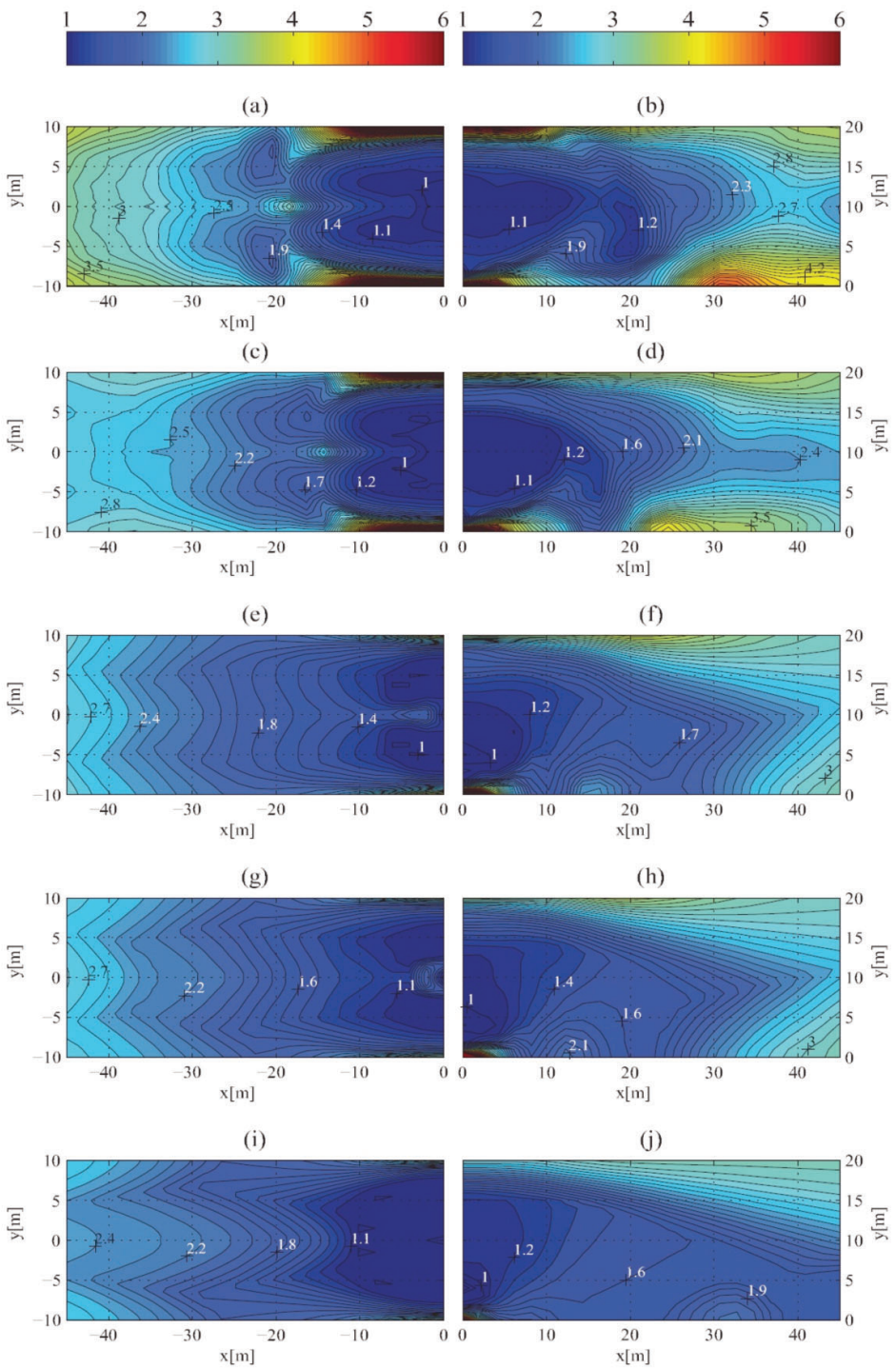

Figure 11. *IA* maps, streets 20 meters wide: a) and b) 10,000 kg of TNT; c) and d) 5,000 kg of TNT; e) and f) 1,000 kg of TNT; g) and h) 500 kg of TNT; i) and j) 100 kg of TNT

6. CHANNELLING ZONES

An explosion in a confined environment proceeds in different stages. In each of these stages, incident and reflected waves may or may not be combined, depending on the geometry and the amount of explosive involved. The amount of explosive determines the speed and intensity of the incident waves. In a similar way, speed differences between the incident and reflected waves increase with the amount of explosive. Then, increasing the amount of TNT produces the effect of "slight elongation" in the *PA* and *IA* maps.

6.1 SYMMETRIC EXPLOSION BEHAVIOURS

To more clearly describe the different stages of a confined explosion, the development of symmetric explosions is shown in Figure 12.

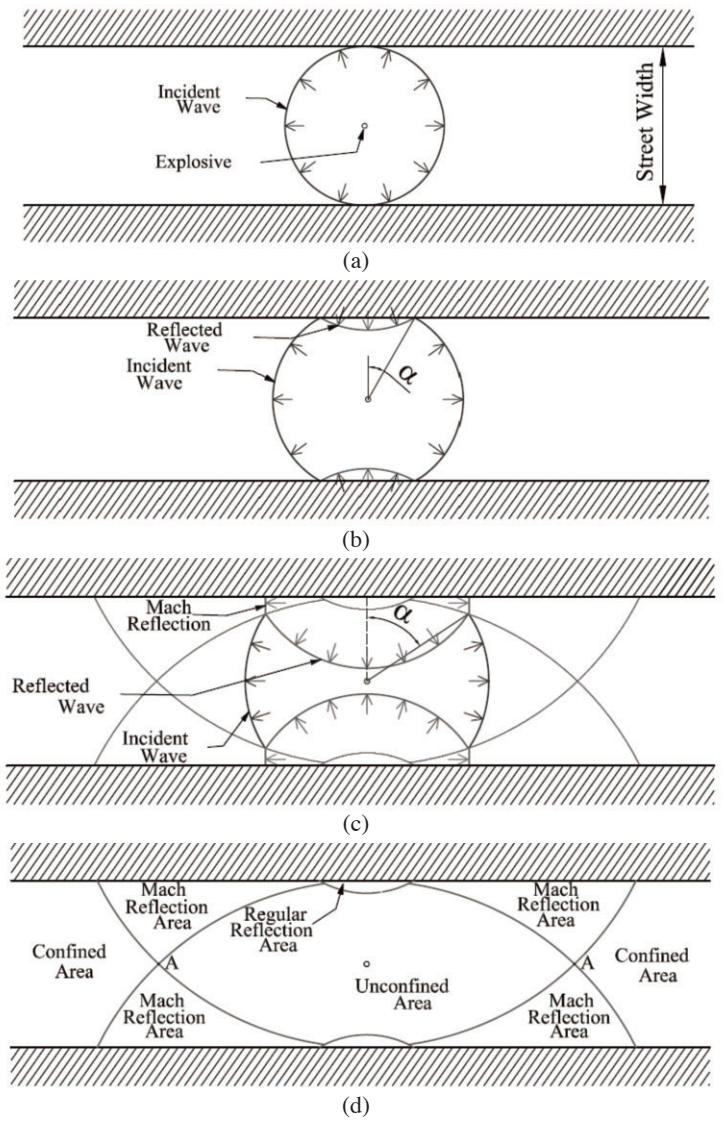

Figure 12. Development of shock waves and definition of channelling zones for symmetric explosions

Figure 12.a shows the shock wave before it reaches the nearest building façade. At this stage, the wave behaves as a two-dimensional explosion. The shock wave then strikes both fronts at once. The normal reflection wave is produced with a reflection factor of C_r (UFC 3-340-02 [1]), which is dependent on the intensity of the incident wave and the angle of incidence. This initial stage of reflection can be observed in Figure 12.b. With the propagation of the incident wave over the façade, angle *a* increases. When *a* reaches a critical value, the Mach reflection is produced. This stage is shown schematically in Figure 12.c. Mach stems are simultaneously formed on both sides of the street. The Mach wave front moves parallel to the axis of the façade with a higher pressure and velocity than the incident shock wave. Finally, both Mach stems intersect at a point above the axis of the street. This occurs approximately at 1.65 times the width of the street. In this work, this point A is called the *"quadruple point"*. Four different channelling zones can thereby be distinguished (Figure 12.d). To explain what happens in each area, a symmetric explosion is used as an example (Figure 13).

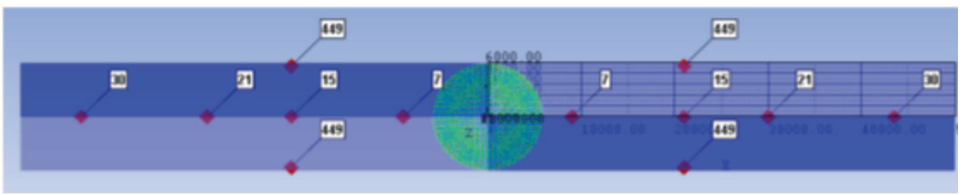

(a)

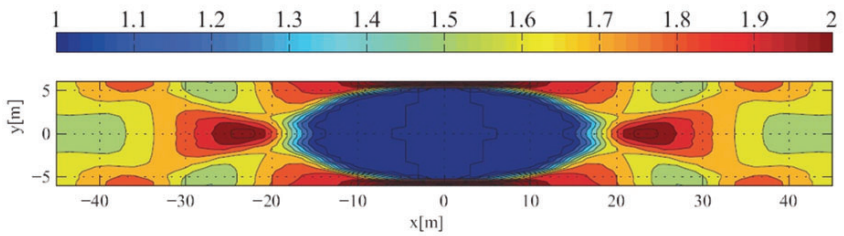

(b)

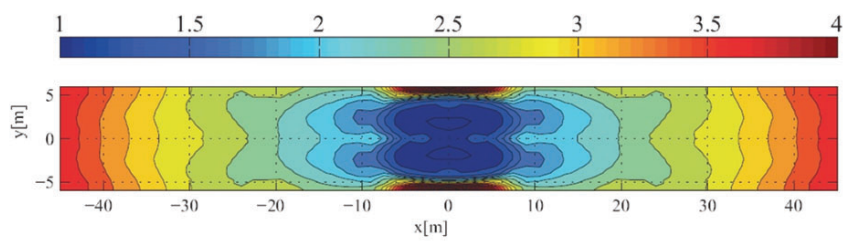

(c)

Figure 13. Street 12 meters wide, symmetric explosion of 1000 kg of TNT: a) Model and gauges; b) Maximal overpressure amplification; c) Maximal impulse amplification

Figure 13.a shows that gauge 7 is located within the unconfined overpressure area. Gauge 15 is near the *quadruple point*, and gauges 21 and 30 are located within the confinement area. Finally, gauge 449 is located within the *Mach Reflection Area*. Figure 14 shows the record of gauge 15, which is very close to the quadruple point and is thus representative of the behaviour at this point. At this point, the incident and reflected waves from the two façades arrive simultaneously. This produces a combined wave front of greater intensity than the individual waves. It can be seen a significant increase in the maximum value of the overpressure as well as the impulse. The shock wave reaches this point at the same time for either confined or unconfined blast waves.

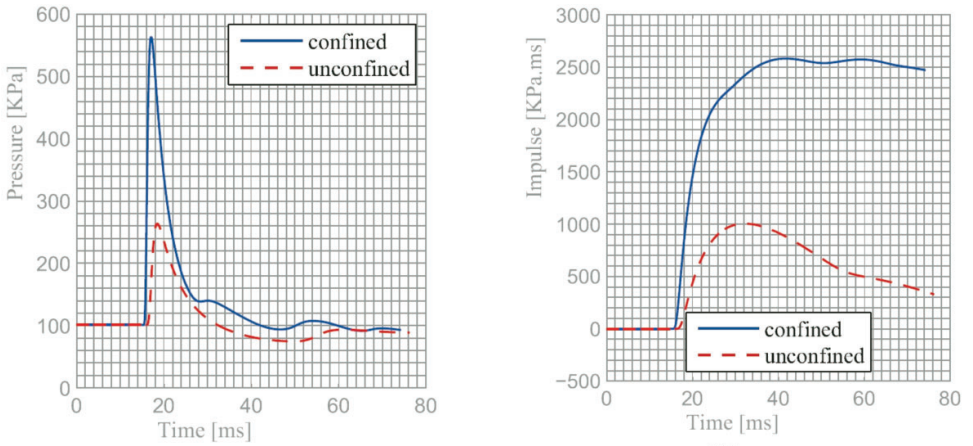

(a) (b)

Figure 14. Time histories of overpressures and impulses. Gauge 15. Quadruple point

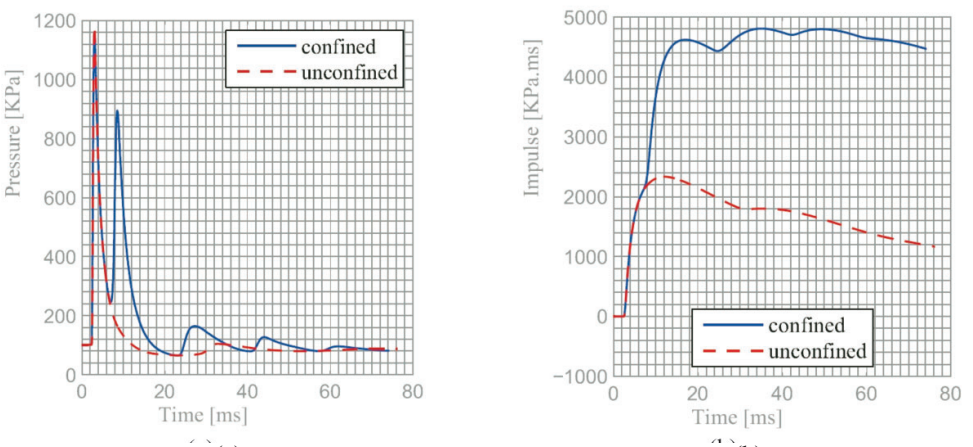

(a) (b)

Figure 15. Time histories of overpressures and impulses. Gauge 7. Unconfined Area

The overpressures and impulses recorded at gauge 7 are shown in Figure 15, which is located in the *Unconfined Area*. This gauge is representative of the behaviour throughout the area. The incident shock wave is the first to arrive, then there is a decrease in the wave intensity, and finally, the waves reflected by the façades arrive. These reflected waves are smaller than the incident wave and only contribute to increasing the maximum impulse (Figure 15b). When the gauge is closer to the explosive, there is a smaller increase in the impulse. On the axis of the explosive, the impulse amplification value is close to 1.

Gauges 21 and 30 are in the *Confined Area*, and the values recorded at these gauges are shown in Figure 16 and Figure 17, respectively. For the gauges located in this zone, a combined wave front of the incident and reflected waves arrives first. The wave arrival time in the confined explosion is substantially earlier than that of the equivalent unconfined explosion. This wave front has greater overpressure and impulse intensities. For this reason, the channelling effect is very important in this zone.

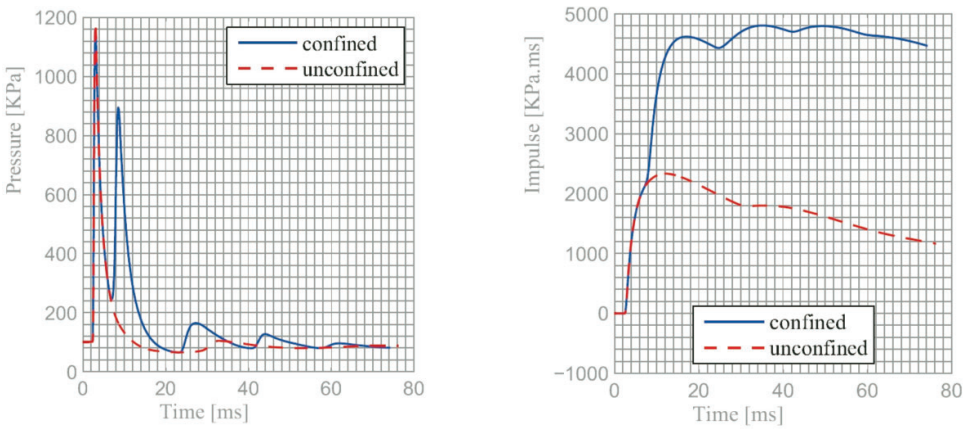

(a) (b)

Figure 16. Time histories of overpressures and impulses. Gauge 21. Confined Area

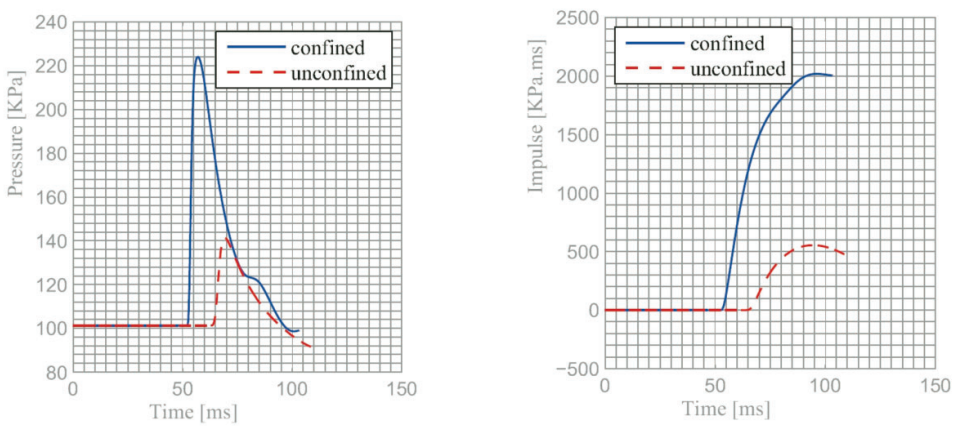

(a) (b)

Figure 17. Time histories of overpressures and impulses. Gauge 30. Confined Area

As shown in Figure 13, gauge 449 is located near the façade in the *Mach Reflection Area*. The records of this gauge are shown in Figure 18. In this zone, the Mach wave is the first to arrive at the gauge. Obviously, this wave front is stronger than the unconfined explosion and generates the maximum recorded overpressure value. Another important feature of this area is that the reflected waves from the opposite façade reach these gauges in a very weak form. For this reason, these reflected waves do not affect the maximum pressure value, and their contribution to the maximum impulse can be neglected.

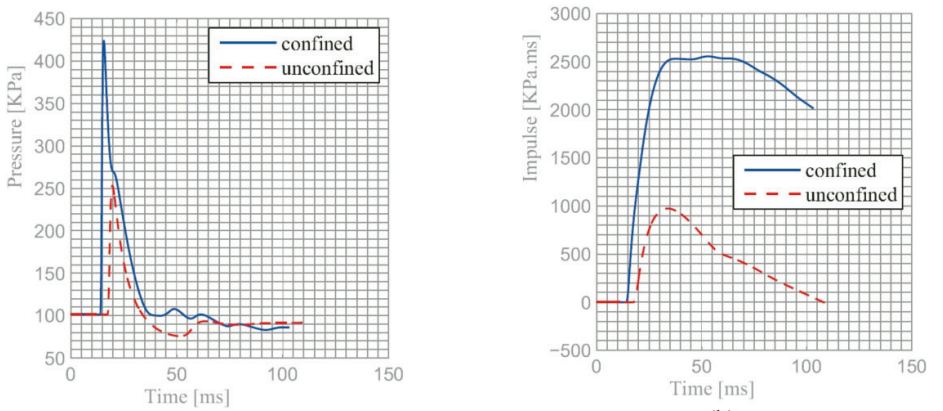

(a) (b)

Figure 18. Time histories of overpressures and impulses. Gauge 449. Mach Reflection Area

6.2 ASYMMETRIC EXPLOSION BEHAVIOURS

The different stages of an asymmetric explosion are presented in Figure 19. Figure 19.a) shows the shock wave before reaching the nearest building façade. At this stage, the wave behaves as a two-dimensional explosion. After that, the shock wave hits the nearest façade, generating a regular reflection on it. As in the case of a symmetrical explosion, a Mach reflection is generated with increasing a (Figure 19.c). As shown in this figure, in the asymmetric explosion, the distance between the explosive and the façades is different. This leads to a different development of the Mach Stem (UFC 3-340-02 [1]). The Mach Stem of the nearest façade grows faster than the farther façade (Figure 19.e). For this reason, *quadruple point* A is located besides the street axis. The same four different channelling zones can also be distinguished (Figure 15.f).

Finally, the behaviour in the *Regular Reflection Area* when the wave front hits the façade with a=0 is also of interest. In this case, an asymmetric explosion of 500 kg of TNT in a street 20 m wide is taken as an example (Figure 20). The *Regular Reflection Area* limits with the *Unconfined Area* in a narrow region.

It is clear that gauges 461 and 438 are located in the *Regular Reflection Area*. In contrast, gauge 323 is located in the *Unconfined Area*. The overpressure and impulse records corresponding to gauge 461 are shown in Figure 21. This gauge is located on the axis of the façade and therefore captures the effects of regular reflection of the wave. The amplification generated by the reflection of the wave on the façade increases both the overpressure and the impulse.

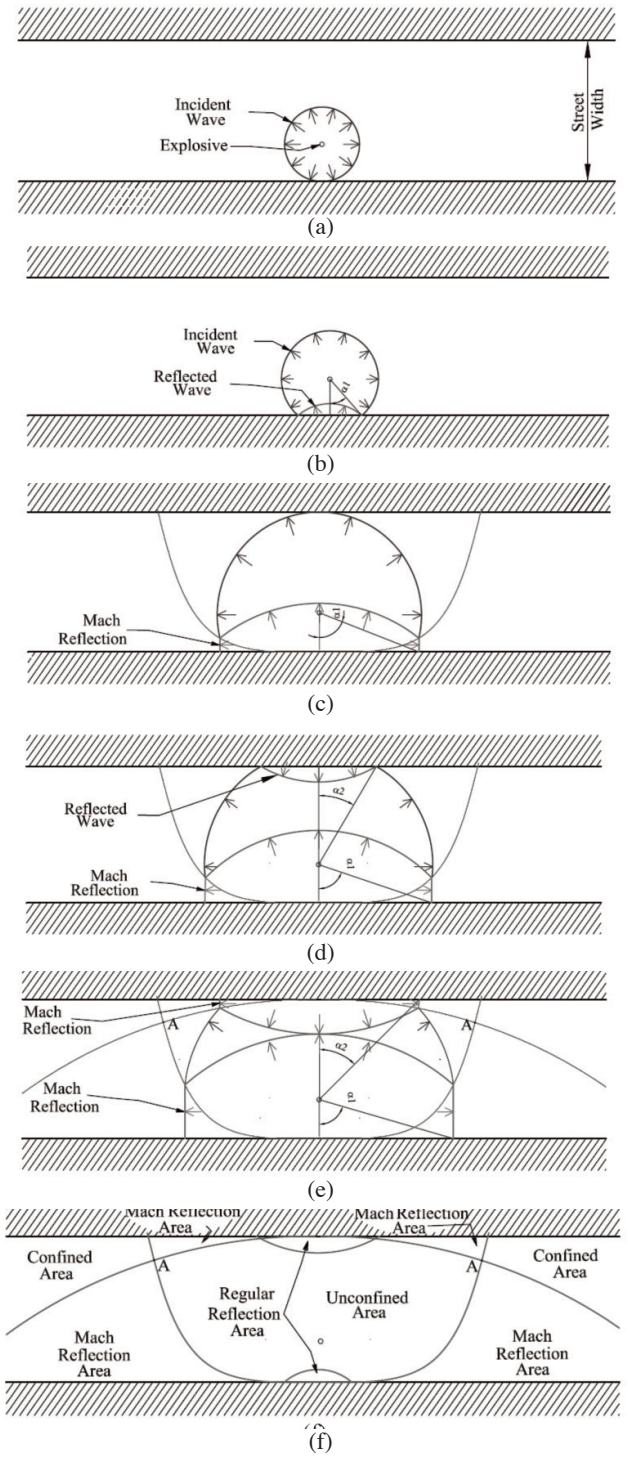

Figure 19. Development of shock waves and definition of channelling zones for asymmetric explosions

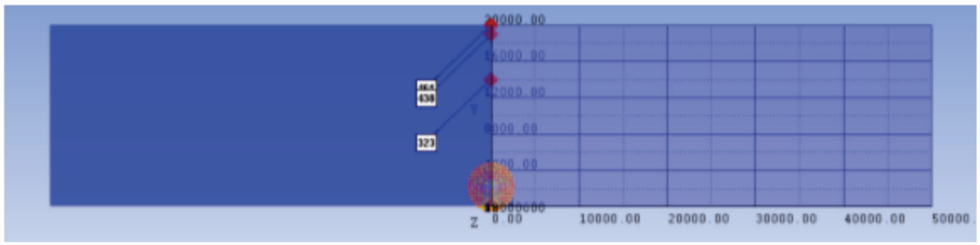

(a)

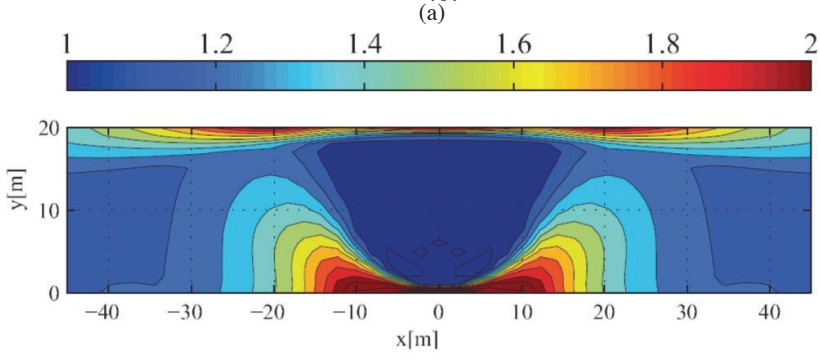

(b)

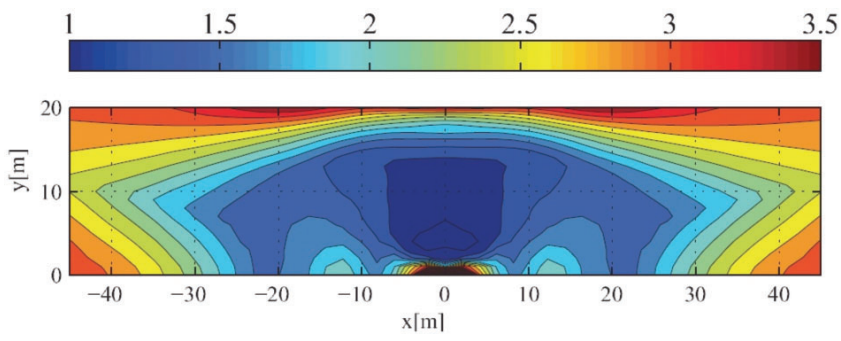

(c)

Figure 20. Street 20 meters wide, asymmetric explosion of 500 kg of TNT: a) Model and gauges; b) Maximal overpressure amplification; c) Maximal impulse amplification

Gauge 438 is located near the façade in the zone of influence of normal reflection. The record for this gauge is shown in Figure 22. In this zone, the incident wave front arrives, and the reflected wave front arrives shortly thereafter. Due to the short distance from the façade, the reflected wave is greater than the incident wave. Therefore, the maximum recorded overpressure is due to the reflected wave. As shown in Figure 22, the overpressure amplification is not very large because the peaks of the incident and reflected waves do not overlap. However, the impulse is greatly increased compared to that of the unconfined explosion.

The intensity of the reflected wave decreases exponentially with increasing distance from the façade. In a short distance from the façade, the incident wave exceeds the reflected wave, which is the case for gauge 323 shown in Figure 23.

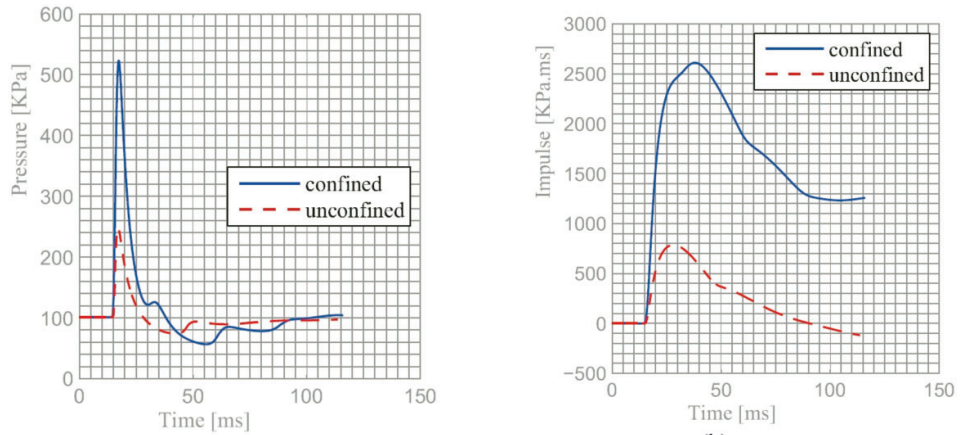

Figure 21. Time histories of overpressures and impulses. Gauge 461. Regular Reflection Area

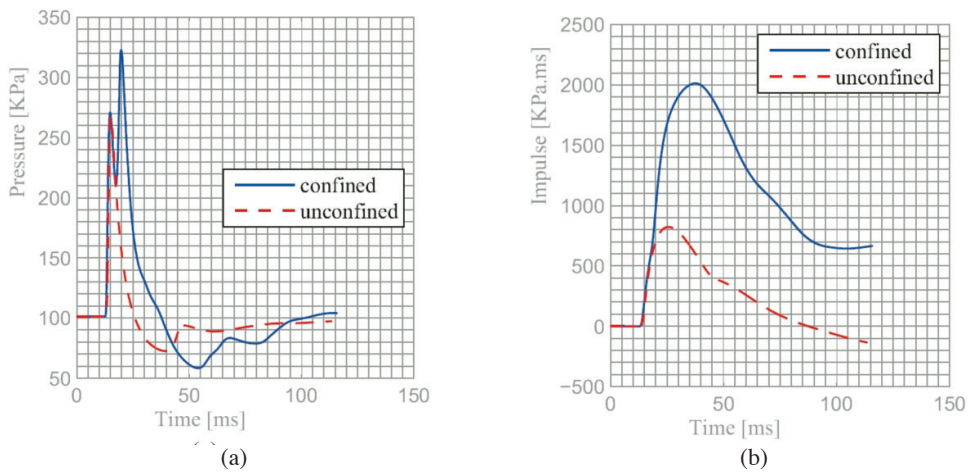

Figure 22. Time histories of overpressures and impulses: a) Gauge 438; b) Regular Reflection Area

The maximum pressure values for both gauges 323 and 7 from the asymmetrical and symmetrical cases are caused by the incident shock wave. All the gauges from this unconfined area have the same characteristics. The reflected waves that arrive later only increase the value of the impulse in this area. The channelling of explosions generates significant increases in the overpressure and/or impulse. In the proximity of the explosive, there are no combinations of waves. This leads to the maximum recorded overpressure, which always corresponds to the incident wave. Moreover, the channelling effect generates an increase in the impulse.

This parametric study shows that the channelling zone areas in Figure 12 and Figure 19 strongly depend on the width of the street and the position of the explosive. This is clarified in Figure 6 to Figure 8 for overpressure amplification and in Figure 9 to Figure 11 for

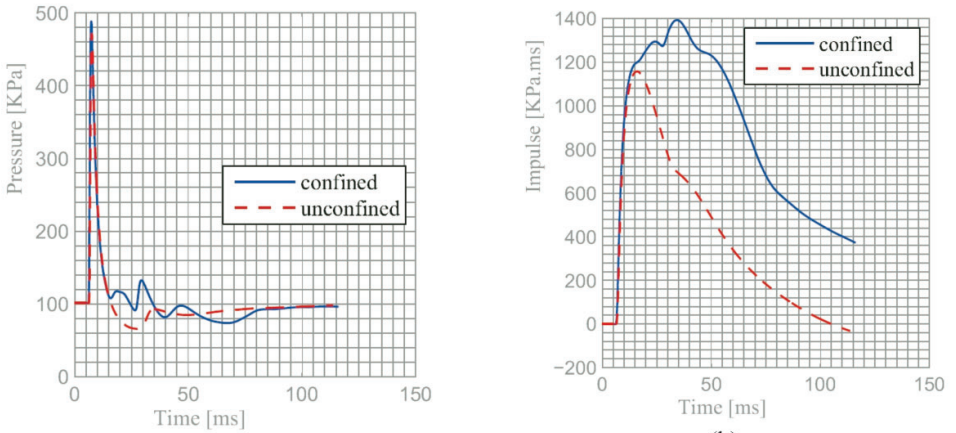

Figure 23. Time histories of overpressures and impulses. Gauge 323. Unconfined Area

impulse amplification. The amount of explosive does not significantly change the position of quadruple point A or the shape or size of the channelling zones.

On the other hand, the amplification factors for both overpressure and impulse obviously increase with the amount of explosive.

7. BEHAVIOUR OF SHOCK WAVES IN CONFINED SPACES

If the street is sufficiently long, the explosion gradually transforms into a planar explosion. Figures 24 and 25 show this process for symmetric and asymmetric explosions. The decay law for a planar explosion is smaller than for the equivalent unconfined explosion. For this reason, there is an effect of channelling on the overpressure and impulse compared to the unconfined explosion. This effect is noticeable for the 6-m street width for loads of 100, 500 and up to 1,000 kg for both the symmetric and asymmetric explosions. If the amount of explosive is increased, a greater distance is required to reach this state. In a similar way, as the street becomes wider, the distance required to reach the equilibrium state increases.

Figures 24 and 25 show the developed channelling effect versus time for both the symmetric and asymmetric explosions. As the explosion takes place, the areas swept by the Mach wavefronts increase. A key point occurs when both Mach wavefronts overlap, generating the quadruple point A. In the symmetrical explosion, this phenomenon occurs at 9.527 m, while in the asymmetrical explosion, it occurs at 6.798 m from this point along the street, generating the unconfined areas.

8. CONCLUSIONS

A parametric study of explosions in urban environments is performed to develop a better understanding of the effects of channelling in congested urban environments. The effects of channelling on streets of different width and with different amounts and locations of explosive are studied. Additionally, the effects of channelling on design parameters such as overpressures and impulses, which are usually used to estimate the destructive potential of an explosion, are discussed.

The channelling effect on the maximum overpressure is mainly generated by the sum of

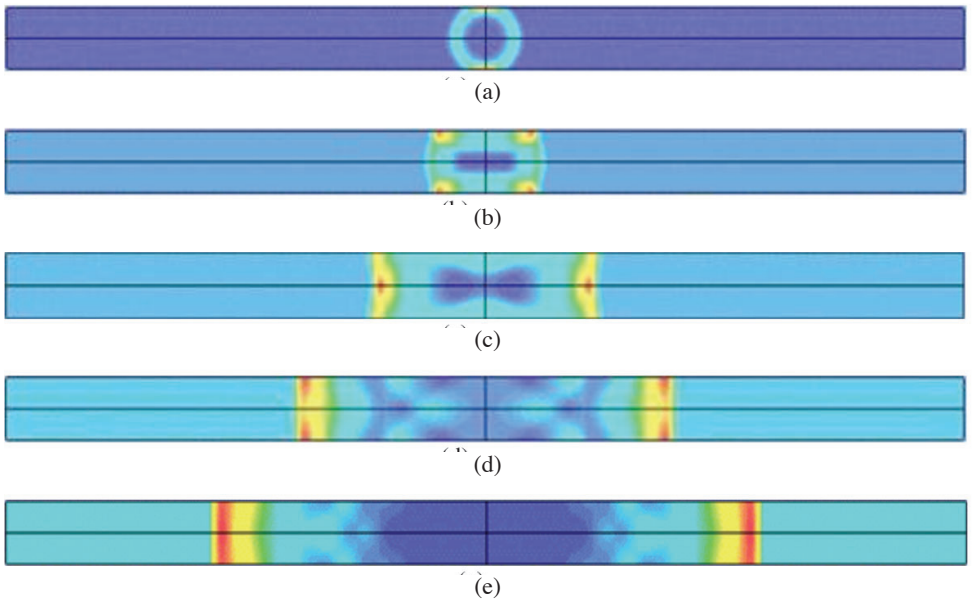

Figure 24. Overpressure blast wave on a street 6 meters wide with a symmetric explosion of 100 kg of TNT: a) 0.4556 m; b) 2.306 m; c) 9.527 m; d) 24.49 m; e) 42 m

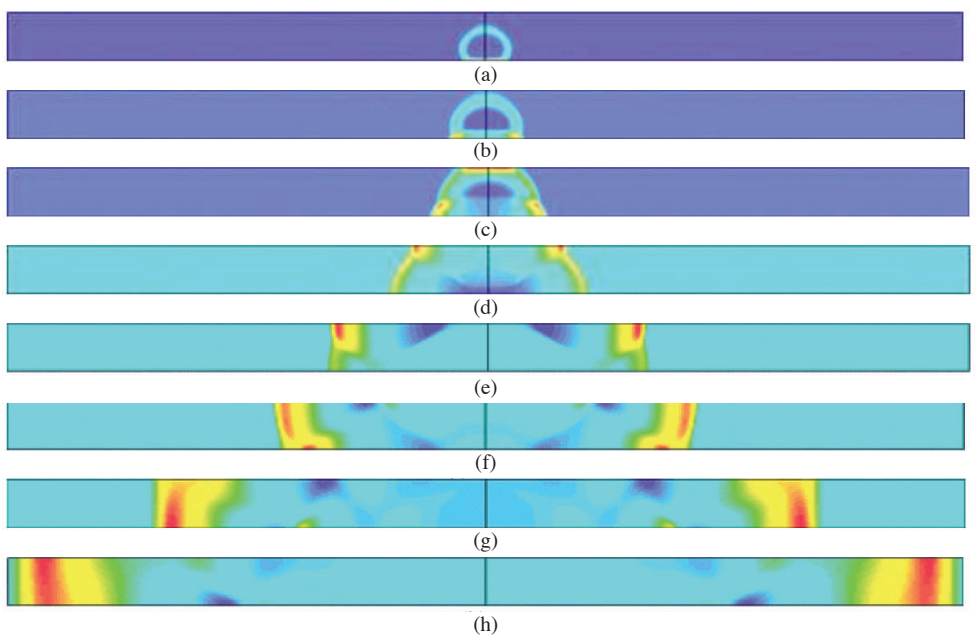

Figure 25. Overpressure blast wave on street 6 meters wide with an asymmetric explosion of 100 kg of TNT: a) 0.6496 m; b) 1.439 m; c) 2.535 m; d) 6.798 m; e) 17.68 m; f) 27.91 m; g) 55.64 m; h) 89.99 m

the incident and reflected waves at the same point and at the same time. In contrast, the impulse of the shockwave is increased by confinement, even without overlapping waves. For this reason, the *PA* maps are different from the *IA* maps.

The study allows presenting the channelling effects in a novel way using maps of overpressures and impulse amplification. These charts could be used as a first approximation for design purposes. In most papers in the literature, it is not distinguished whether the enhancement of the overpressures and impulses is produced by reflection, Mach effect or channelling itself. In this paper, four types of zones were defined where the channelling effects are different, and the characteristics of each zone are discussed. These four areas are observed in both symmetric and asymmetric explosions. In this work, the zones were named in this work as *Unconfined Area*, the *Regular Reflection Area*, the *Mach Reflection Area* and the *Confined Area*. Moreover, the common point among the four areas is defined as *quadruple point*. The channelling zones only depend on the width of the street and the location of the explosive.

The analysis of the effects of an asymmetric explosive charge located at 2.20 meters from one of the façades on the channelling phenomenon has particular importance. To the best of our knowledge, this is the first description of the influence of an asymmetrical blast load on the overpressures and impulses of a city street. This case is important because many terrorist attacks are perpetrated by parking a car bomb in front of a target building.

If the street is long enough, the explosion gradually transforms into a planar explosion. The decay law of a planar explosion is smaller than that of an equivalent unconfined explosion. If the amount of explosive or the width of the street is increased, a greater distance is required to reach this state.

The following conclusions can be drawn regarding the main variables studied:

a) Amount of explosive

- The amount of explosive does not significantly change the position of the *quadruple point* or the shape or size of the channelling zones.
- The amplification factor of overpressures and impulses increases with the amount of explosive, as expected.
- For the *Confined Area*, the coefficient *PA* is increased by roughly 4, 3.5 and 2.5 times for the street widths of 6 m, 12 m and 20 m, respectively, when increasing the amount of TNT from 100 kg to 10,000 kg.
- For the *Confined Area*, the coefficient *IA* is increased by roughly 1.5 times when increasing the amount of TNT from 100 kg to 10,000 kg for all street widths.

b) Width of the street

- The location, extent and shape of the different channelling zones are strongly dependent on the street width.
- When the street is wider, the amplification factors are reduced along the street.
- For the *Confined Area*, the coefficient *PA* is reduced by roughly 3 and 2 times for 10,000 kg and 100 kg of TNT, respectively, when increasing the street width from 6 m to 20 m.
- For the *Confined Area*, the coefficient *IA* is reduced by roughly 2.4 times for 10,000 kg and 100 kg of TNT when increasing the street width from 6 m to 20 m.
- Both Mach stems intersect at a point above the axis of the street. This occurs at approximately 1.65 times the width of the street (the quadruple point). Therefore, if the street is more than 30 m wide, the confined zone will not appear in the typical block.

c) Location of the explosive (symmetric or asymmetric)

- In the case of asymmetric explosions, the *quadruple point* is closer to the farthest façade. Therefore, the location of the explosive greatly affects the configuration of the different zones of confinement.
- In the case of asymmetric explosions, the amplification factors are greater than in the symmetrical explosions close to the *quadruple point* and in the *Confined Area* for the same street width and the same amount of explosive.

In summary, because overpressures and impulses can be increased up to 8 times in the *Confined Area*, channelling is a phenomenon that can significantly increase the destructive potential of the shock wave of an explosion. Hence, this factor must be taken into account in the design of structures that may be subjected to this type of extreme load in congested urban environments.

ACKNOWLEDGMENTS

The financial support of CONICET (Argentina) and SECYT (National University of Cuyo) is gratefully acknowledged. Special acknowledgements are extended to the reviewers of the first version of the paper because their useful suggestions led to improvements of this work.

REFERENCES

[1] US Department of the Army, *Structures to Resist the Effects of Accidental Explosions*, US Army Corps of Engineer, UFC 3-340-02, 2008.UFC 3-340-02.

[2] US Department of the Army. *Fundamentals of Protective Design for Conventional Weapons*. Department of the Army. Technical Manual TM5- 855-1, 1985

[3] Hyde, D.W., *ConWep – Conventional Weapons Effects*. Department of the Army, Waterways Experiment Station, US Army Corps of Engineers, PO Box 631, USA,1992

[4] Baker W. Cox P.,Westine P.,Kulesz J., and Strehlow R., *Explosion Hazards and Evaluation* , Elsevier ,Amsterdam, 1983.

[5] Smith P. D. & Hetherington JG., *Blast and Ballistic Loading of Structures*, Butterworth-Heinemann, Oxford, 1994.

[6] Cormie D., Mays GC., Smith PD., *Blast Effects on Buildings*, 2nd edn., Thomas Telford, London, 2009.

[7] Clutter, J. K., Mathis, J. T., & Stahl, M. W., Modeling environmental effects in the simulation of explosion events, *International journal of impact engineering*, 2007, 34(5), 973-989.

[8] Johansson, M., Larsen, O. P., Laine, L., & AB, R. S., Explosion at an intersection in an Urban Environment–Experiments and analyses, in: *Proceedings of the 78th Shock and Vibration Symposium,* Philadelphia, PA, USA, 2007.

[9] Larcher, M., & Casadei, F., Explosions in complex geometries-a comparison of several approaches, *International journal of protective structures*, 2010, 1(2), 169-196.

[10] Alia, a., & Souli, M., High explosive simulation using multi-material formulations, *Applied Thermal Engineering*, 2006, 26(10), 1032-1042.

[11] Alhussan, K., Stepanov, K. L., Stankevich, Y. A., Smetannikov, A. S., & Zhdanok, S. A., Hydrodynamics of the initial phase of explosion, *International Journal of Heat and Mass Transfer,2011,* 54 1627–1640

[12] Lu, Y., Wang, Z., & Chong, K., A comparative study of buried structure in soil subjected to blast load using 2D and 3D numerical simulations. *Soil Dynamics and Earthquake Engineering*, 2005, 25(4), 275-288.

[13] Wang, Z., Lu, Y., Hao, H., & Chong, K., A full coupled numerical analysis approach for buried structures subjected to subsurface blast. *Computers & Structures*, 2005, 83(4-5), 339-356.

[14] Børvik, T., Hanssen, a. G., Langseth, M., & Olovsson, L., Response of structures to planar blast loads – A finite element engineering approach. *Computers & Structures*, 87(9-10), 2009, 507-520.

[15] Luccioni, B., Ambrosini R.D., Danesi R.F., Analysis of building collapse under blast loads. *Engineering Structures*, 2004, 26(1), 63-71.

[16] Rose T.A., Smith P.D., Influence of the principal geometrical parameters of straight city streets on positive and negative phase blast wave impulses. *International Journal of Impact Engineering 27* , 2002, 359–376.

[17] Trelat, S., Sochet, I., Autrusson, B., Loiseau, O., & Cheval, K., Strong explosion near a parallelepipedic structure, *Shock Waves*, 2007, 16(4-5), 349-357.

[18] Zyskowski, A., Sochet, I., Mavrot, G., Bailly, P., & Renard, J., Study of the explosion process in a small scale experiment-structural loading. *Journal of Loss Prevention in the Process Industries*, 2004, 17(4), 291-299.

[19] Rigas, F., & Sklavounos, S., Experimentally validated 3-D simulation of shock waves generated by dense explosives in confined complex geometries, *Journal of hazardous materials*, 2005, *121*(1), 23-30.

[20] Benselama, A. M., William-Louis, M. J.-P., & Monnoyer, F., Prediction of blast wave effects on a developed site, *International Journal of Impact Engineering*, , 2010, 37(4), 385-396.

[21] Silvestrini, M., Genova, B., & Leon Trujillo, F. J., Energy concentration factor. A simple concept for the prediction of blast propagation in partially confined geometries, *Journal of Loss Prevention in the Process Industries*, 2009, 22(4), 449-454.

[22] Remennikov, AM, A Review of Methods for Predicting Bomb Blast Effects on Buildings, *Journal of Battlefield Technology*, 2003, 6(3) 5-10.

[23] Remennikov A.M., & Rose, T., Modelling blast loads on buildings in complex city geometries, *Computers & Structures*, 2005, 83(27), 2197-2205.

[24] Smith, P. D., & Rose, T. A., Blast wave propagation in city streets-an overview, *Progress in Structural Engineering and Materials*, 2006, 8(1), 16-28.

[25] Fairlie GE, Johnson NF, Moran KC., Validated numerical simulations of blast loads on structures, in: *The 16th international symposium on military aspects of blast and shock*, 2000.

[26] Ambrosini, D., Luccioni, B., Jacinto, A., & Danesi, R., Location and mass of explosive from structural damage, *Engineering Structures*, 2005, 27(2), 167-176.

[27] Luccioni, B., Ambrosini, D., & Danesi, R., Analysing explosive damage in an urban environment, *Proc. of the Inst. of Civil Eng.: Structures and Buildings*, 2005. 158(1), 1-12.

[28] FEMA 426, Reference Manual to Mitigate Potential terrorist attacks against Buildings, Department of Homeland Security, U.S., 2003.

[29] Codina, R., *Determination of confinement effects in urban environments subjected to blast loading*. Master Thesis (in Spanish). Engineering Faculty, University of Cuyo, Argentina, 2012

[30] ANSYS-AUTODYN., *Interactive Non-Linear Dynamic Analysis Software*, Version 12.1.0, User´s Manual. Century Dynamics Inc, *2009*.

[31] Lee, E. L., & Tarver, C. M., Phenomenological model of shock initiation in heterogeneous explosives, *Physics of Fluids*, 1980, *23*, 2362.

[32] Luccioni, B., Ambrosini, D., & Danesi, R., Blast load assessment using hydrocodes. *Engineering Structures*, 2006, 28(12), 1736-1744.

[33] Zhou, X. Q., & Hao, H., Prediction of airblast loads on structures behind a protective barrier, *International Journal of Impact Engineering*, 2008, 35(5), 363-375.

[34] Benselama, A. M., William-Louis, M. J.-P., & Monnoyer, F., A 1D–3D mixed method for the numerical simulation of blast waves in confined geometries*, Journal of Computational Physics*, 228(18), 2009, 6796-6810

[35] Baum J.D., E.L. Mestreau, H. Luo, R. Lohner, D. Pelessone, C. Charman, M.E. Giltrud & Y. Sohn. Coupling of CFD and CSD methodologies for modelling blast and structural response. In: *Advances in fluid mechanics fluid structure interaction II*, vol. 36, 2003. p. 329–341.

[36] Smith, P. D., & Rose, T. A., Blast loading and building robustness, *Progress in Structural Engineering and Materials*, 2002, 4(2), 213-223.

[37] Smith, P.D., Rose, T.A., Krahe, S.L., Franks, M.A., Façade failure effects on blast propagation along city streets, *Proceedings of the Institution of Civil Engineers: Structures and Buildings*, 2003, 56 (4), 359-365.